Nanoscale

PAPER

View Article Online
View Journal | View Issue

Cite this: *Nanoscale*, 2017, **9**, 6748

High-efficiency inverted quantum dot light-emitting diodes with enhanced hole injection†

Lishuang Wang,[a,b] Ying Lv,[a] Jie Lin,*[a] Yi Fan,[a] Jialong Zhao,*[c] Yunjun Wang[d] and Xingyuan Liu*[a]

Received 26th February 2017,
Accepted 18th April 2017

DOI: 10.1039/c7nr01414g

rsc.li/nanoscale

Hybrid MoO_3/HAT-CN is employed as a hole injection layer (HIL) in green inverted colloidal quantum dot light-emitting devices (QLEDs). The hybrid HILs can be easily prepared and have been found to effectively improve the electroluminescent properties. The best performance device had an HIL of 1.5 nm-thick MoO_3/2.5 nm-thick HAT-CN and showed a turn-on voltage of 1.9 V, a maximum current efficiency (CE_{max}) of 41.3 cd A^{-1}, and maximum external quantum efficiency of 9.72%. Compared to the corresponding devices with the single MoO_3 or HAT-CN interlayer, the CE_{max} of the hole-only devices was improved by 1.6 or 1.5 times, respectively. The measured electrical performance shows that hole-only devices with hybrid HILs have a smaller leakage current density at low driving voltage and much enhanced hole injection current than the devices with single interlayers. It indicates that much improved electroluminescent efficiency in green inverted QLEDs with hybrid MoO_3/HAT-CN orginates from the significant enhancement of hole injection efficiency and suppression of space charge accumulation in the quantum dot-emitting region due to the improved balance of the charge carriers. The hybrid HILs can be extended to other color inverted QLEDs, which are favorable to achieve bright, highly efficient, and color saturation devices for display applications.

Introduction

Colloidal quantum dot light-emitting diodes (QLEDs) have become the most potential candidates for the next-generation display and solid-state lighting technologies because of their important advantages such as size-controllable emission wavelength tunability, narrow linewidth, and solution-processed fabrication.[1–4] Since the first report of QLED,[5] remarkable progress has been made based on the fast development of synthesis strategy (thick shell,[6–8] alloy-intermediate shell,[9,10] and organic ligands[11]), device architecture (conventional[12,13] and inverted[3,14]), and interfacial engineering.[15] Especially, *via* utilizing proper electrode interlayers (organic,[16] inorganic,[17] and hybrid[18]) to adjust the charge injection, transport, and recombination property, the performance of QLEDs was found to be gradually close to that of mature organic light-emitting diodes (OLEDs).

As for the cathode buffer layer, ZnO nanoparticles (NPs) are the most widely used material due to their efficient electron injection and transport property and they match the energy level engineering of the hole transport layer (HTL) of conventional organic materials. A series of red, green, and blue QLEDs, which exhibited high stability and long operating lifetimes, were obtained with the incorporation of ZnO NPs.[4] A record luminance of 218 800 cd m^{-2} in the green inverted QLEDs was reported using the ZnO NPs as the electron transport layer (ETL).[1] However, the maximum current efficiency CE of 19.2 cd A^{-1} and external quantum efficiency (EQE) of 5.8% of this inverted device was still lower than those of conventional devices.[8,16,19] In addition, recent studies show that the strong electron injection ability of ZnO NPs layer can cause injection of excess electrons into the QD active layer and subsequently form undesirable leakage current. This can lead to charged excitons and then the reduction of electroluminescence (EL) performance due to auger recombination. One way to solve the abovementioned problem is by virtue of the reduction of excess carriers injecting into the QD layer and forming efficient exciton recombination. This idea was previously demonstrated using a thin poly(methyl methacrylate) (PMMA) insulating layer that was sandwiched between the ZnO NPs and QDs or double aluminium oxide (Al_2O_3) interlayer around

[a]*State Key Laboratory of Luminescence and Applications, Changchun Institute of Optics, Fine Mechanics and Physics, Chinese Academy of Sciences, Changchun 130033, China. E-mail: linj@ciomp.ac.cn, liuxy@ciomp.ac.cn*
[b]*University of Chinese Academy of Sciences, Beijing 100049, China*
[c]*Key Laboratory of Functional Materials Physics and Chemistry of the Ministry of Education, Jilin Normal University, Siping 136000, China. E-mail: zhaojl@ciomp.ac.cn*
[d]*Suzhou Xingshuo Nanotech Co., Ltd (Mesolight), Suzhou 215123, China*
†Electronic supplementary information (ESI) available. See DOI: 10.1039/c7nr01414g

QDs for high-efficiency and long lifetime QLEDs.[20,21] However, all these improvements in EL performance were obtained at the expense of suppressing the excess electrons. Another more desirable approach to circumvent the influence of leakage current is to enhance the injection and transport of minority carriers, holes, to improve the device performance.

High work function transition metal-oxides, such as molybdenum oxide (MoO_3),[7,22] tungsten oxide (WO_3),[18] vanadium oxide (V_2O_5),[23] and deep lying lowest unoccupied molecular orbital (LUMO) organic materials, such as 1,4,5,8,9,11-hexaazatriphenylene-hexacarbonitrile (HAT-CN),[24,25] have been successfully used as electrode buffer layers in QLEDs. Using HAT-CN as an HIL, H. M. Kim *et al.* obtained a high CE of 34 cd A^{-1} in inverted green QLED.[25] Herein, we report the first use of a hybrid MoO_3/HAT-CN HIL for high-performance, green inverted QLEDs. The inverted structure was chosen because it could minimize the electric field, which could induce a spatial separation of the electron and hole wave functions in forward bias,[26,27] thus increasing the radiative rate of excitons. We found that just inserting an ultrathin MoO_3 between 4,4′-bis(carbazole-9-yl)biphenyl (CBP) and HAT-CN layer could remarkably improve the hole injection and dramatically increase the CE and EQE of inverted QLEDs simultaneously. As a result, the best performance device (1.5 nm MoO_3/HAT-CN) exhibited a maximum CE of 41.3 cd A^{-1} and maximum EQE of 9.72%. These peak efficiencies of the hole-enhanced inverted QLEDs are almost 1-time higher than those of the earlier reported green inverted device (maximum CE of 19.2 cd A^{-1} and maximum EQE of 5.8%[1]). This method can be extended to other colored QLEDs and would lead to bright, high-efficiency, and color-saturation devices for display applications.

Results and discussion

The green emitting CdSe@ZnSe/ZnS QDs used in this study exhibited good monodispersity, had a size of 10–12 nm (Fig. S1†), and a photoluminescence (PL) emission peak at 528 nm (Fig. S2†). With the PL quantum yield (QY) of approximately 75% in solution and 34% in the solid state film on glass (Fig. S3 and S4†), the QDs exhibit a stable and highly efficient PL performance, which plays an important role in determining the EL performance of the QLEDs. To investigate the effect of the HIL on the EL characteristics of the QDs, a series of inverted QLEDs was fabricated with the following structure (Fig. 1a): cathode (Indium Tin Oxide, ITO)/ZnO NPs (35 nm)/QDs (15 nm)/CBP (50 nm)/HIL (4 nm, MoO_3, HAT-CN or MoO_3/HAT-CN)/Al, where ZnO NPs, QDs, and CBP served as electron injection and transport layer (EIL/ETL), light-emitting layer (EML), and HTL, respectively. The cross-section SEM image shown in Fig. 1b reveals that each functional layer in

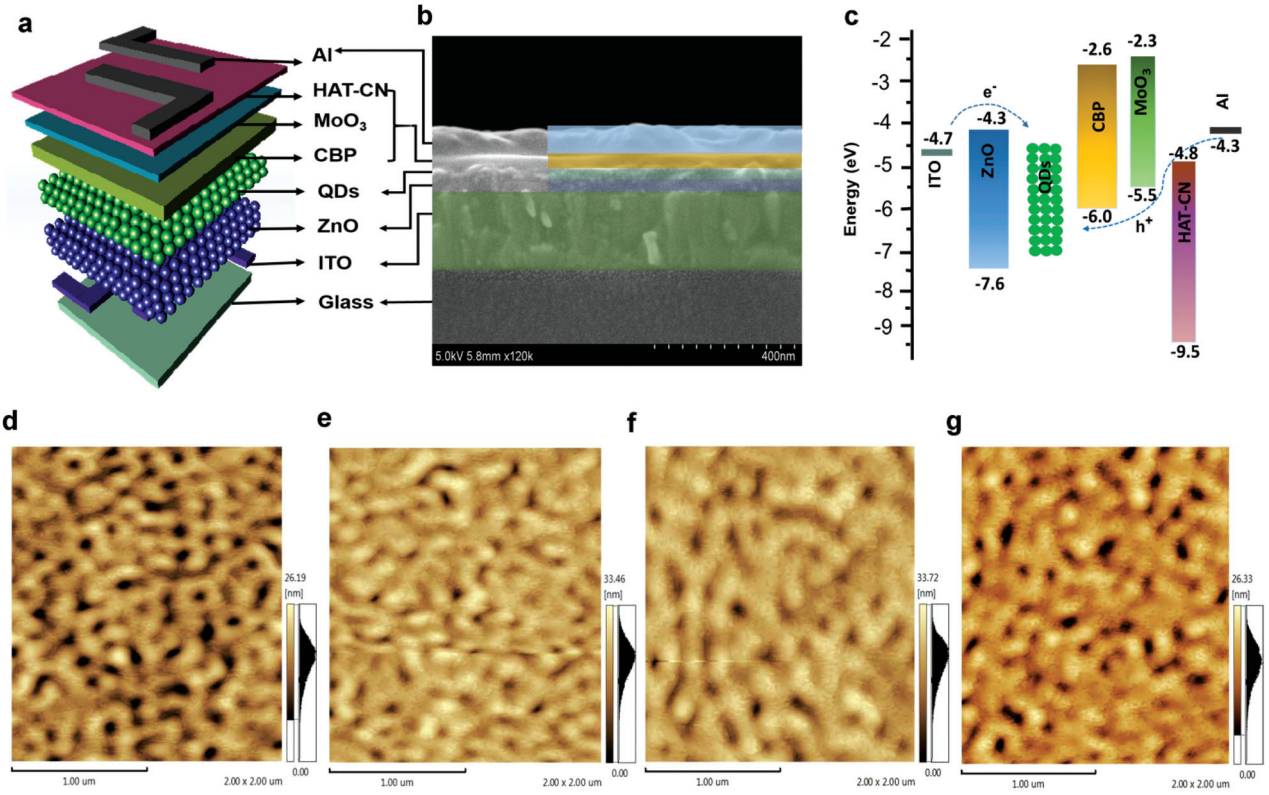

Fig. 1 (a) Architecture of QLED. (b) Cross-sectional SEM image of the representative device. (c) Energy band diagram of QLED. Surface morphology of the multilayer structures with different thicknesses of MoO_3 layer. (d) ITO/ZnO NPs/QDs/CBP/MoO_3 (0 nm). (e) ITO/ZnO NPs/QDs/CBP/MoO_3 (0.5 nm). (f) ITO/ZnO NPs/QDs/CBP/MoO_3 (1.5 nm). (g) ITO/ZnO NPs/QDs/CBP/MoO_3 (2.5 nm).

the device is uniformly formed with a clear interlayer. The energy level diagram of the QLED is illustrated in Fig. 1c. The hybrid buffer layer used in the inverted device presents several advantages: (1) its high work function of MoO_3 matches with the low LUMO of HAT-CN and enhances the hole injection; (2) it can be easily processed *via* thermal evaporation, which can be continuously operated during the device fabrication; and (3) it is conducive to the energy level matching of the highest occupied molecular orbital (HOMO) of HTL and the work function of the metal Al electrode, which is beneficial to the improvement of the EL performance of inverted QLEDs. Surface morphologies of these thin MoO_3 layers were measured and are provided in Fig. S5.† With 0.5 nm MoO_3, the surface roughness of the CBP film increases to 10.058 nm from 8.953 nm, which means that the surface is discontinuous. When the thickness of MoO_3 increases, the surface roughness reduces, which implies that the discontinuity of the surface decreases and forms a comparative smooth surface. Similar results of the devices are shown in Fig. 1d–g; without the MoO_3 layer, the surface roughness of ITO/ZnO NPs/QDs/CBP is 4.562 nm. However, with the MoO_3 layer, the surface roughness of ITO/ZnO NPs/QDs/CBP/MoO_3 (1.5 nm) decreases to 4.403 nm.

Fig. 2 shows the EL performance of QLEDs with single MoO_3, HAT-CN, and hybrid MoO_3/HAT-CN as an HIL. As *J*–*V* characteristics demonstrated in Fig. 2a, the turn-on voltage (V_{on}) of QLED with single MoO_3 and single HAT-CN HIL were 3.4 and 2.5 V, respectively. In contrast, by inserting a 1.5 nm thick MoO_3 layer between the CBP and HAT-CN layer, the V_{on} of this QLED significantly decreased to only 1.9 V. Moreover, obvious decrease in the current density at low driving voltage region ($<V_{on}$) was also realized in these hybrid devices, suggesting a rather small leakage current. The current density of the device with single MoO_3 (device A, black line) at the driving voltage of 0.4 V was 1.1×10^{-2} mA cm^{-2}, which was 1.97 times higher than that of the device with single HAT-CN (device B, red line) (3.7×10^{-3} mA cm^{-2}). Moreover, the difference in the current density values for the two devices slightly changed when the driving voltage was increased at the low bias voltage region (<3 V). However, for devices with hybrid HILs, the leakage current at low driving voltage region (<2 V) exhibited a value more than one order of magnitude lower than those of the devices A and B. When driving voltage was increased, the injection current density of the hybrid HIL device showed the same order of magnitude as that of the device with single HIL (device A and B), which was beneficial for achieving a high EL performance.

As shown in Fig. 2b, the luminance at 1 cd m^{-2} for the devices with hybrid HILs was obtained at the driving voltage below 3.5 V, which was much lower than that of the device A (4.3 V). The maximum luminance for all the QLEDs except for the device E (pink line) was found to be more than 60 000 cd m^{-2}. A slight decrease in the maximum luminance of device E may originate from the larger resistance of the relatively thick MoO_3. However, compared to the devices with a single interlayer, the hybrid devices were operated at smaller driving voltage to obtain the same luminance. As shown in Fig. 2c, a remarkable improvement of CE was achieved by incorporating hybrid HIL into the device structure. It was found that the 1.5 nm-thick MoO_3 layer (device D, blue line) showed the maximum CE of 41.3 cd A^{-1} at the luminance of 11 600 cd m^{-2}, which was approximately 1.6-fold higher than that of device A with single MoO_3 as the interlayer (15.8 cd A^{-1}). For device D, the CE was well maintained within 90% when the luminance was increased to 30 000 cd m^{-2}. It can be seen that with a hybrid HIL, the roll-off in the emission efficiency at high luminance range was less than that of the device A. The CE of device A remained only 80% at the luminance of 30 000 cd m^{-2}.

A simultaneous improvement of EQE was achieved, as shown in Fig. 2d. Maximum EQE of 3.68, 3.88, 6.96, 9.72, and 8.60% were obtained for the devices A, B, C, D, and E, respectively. It was found that the device D with a 1.5 nm MoO_3 layer showed the best EL performance with a quite low leakage current, rather high luminance, and the highest CE and EQE amongst the five devices. As presented in Fig. 2e, due to the interdot interactions and the electric-field-induced Stark effect,[28] the peak wavelength in the EL spectrum of device D, which was at 532 nm, exhibited a 4 nm red-shift. Due to a narrow full-width at half-maximum (FWHM) of 24 nm and Commission Internationale de I'Eclairage (CIE) 1931 color coordinates of (0.221, 0.739) (Fig. 2f), the color-saturation makes this green inverted QLED an ideal green array for display application. EL spectra of device A, B, C, D and E are also shown in Fig. 2e, and it was found that the peak wavelength and FWHM did not change any more and these devices showed similar CIE properties (Fig. 2f).

Detailed EL characteristics of the device A–E are summarized in Table 1, and the EL performance of the devices with different thicknesses of HAT-CN in the hybrid HILs are provided in the ESI (Fig. S6 and Table S1†). It clearly shows that inserting a MoO_3 layer can reduce the accumulation of space charge within the emission region, of which charged QDs reach dark by an ultrafast, auger-mediated decay pathway.[3,29] The great improvement in the EL performance of devices with a hybrid HIL (Fig. 2a–d) implies that charge injection into the QDs layer becomes more efficient. As seen in Fig. 1c, due to the low conduction band (CB) of −4.3 eV and VB of −7.6 eV of ZnO NPs, the electron injection and transport from ITO to QD EML are facilitated. The VB (−5.5 eV) of MoO_3 (Fig. S7†) enables the efficient hole to inject from the LUMO (−4.8 eV)[25] of HAT-CN to the HOMO (−6.0 eV) of CBP. Owing to the benefited systematic engineering of HIL, HTL, and EIL/ETL, the change in the inverted QLED can make effective carrier injection, transport, and recombination.

To understand the influence of hole injection on the *J*–*V* properties as well as EL performance, current densities of different HIL hole-only devices with the structure of ITO/MoO_3 (30 nm)/QDs/CBP/HIL/Al were obtained at different driving voltages. From Fig. 3a, it can be observed that hole current density of the HAT-CN device is larger than that of the MoO_3 device. Using the hybrid HIL, the enhancement of the hole

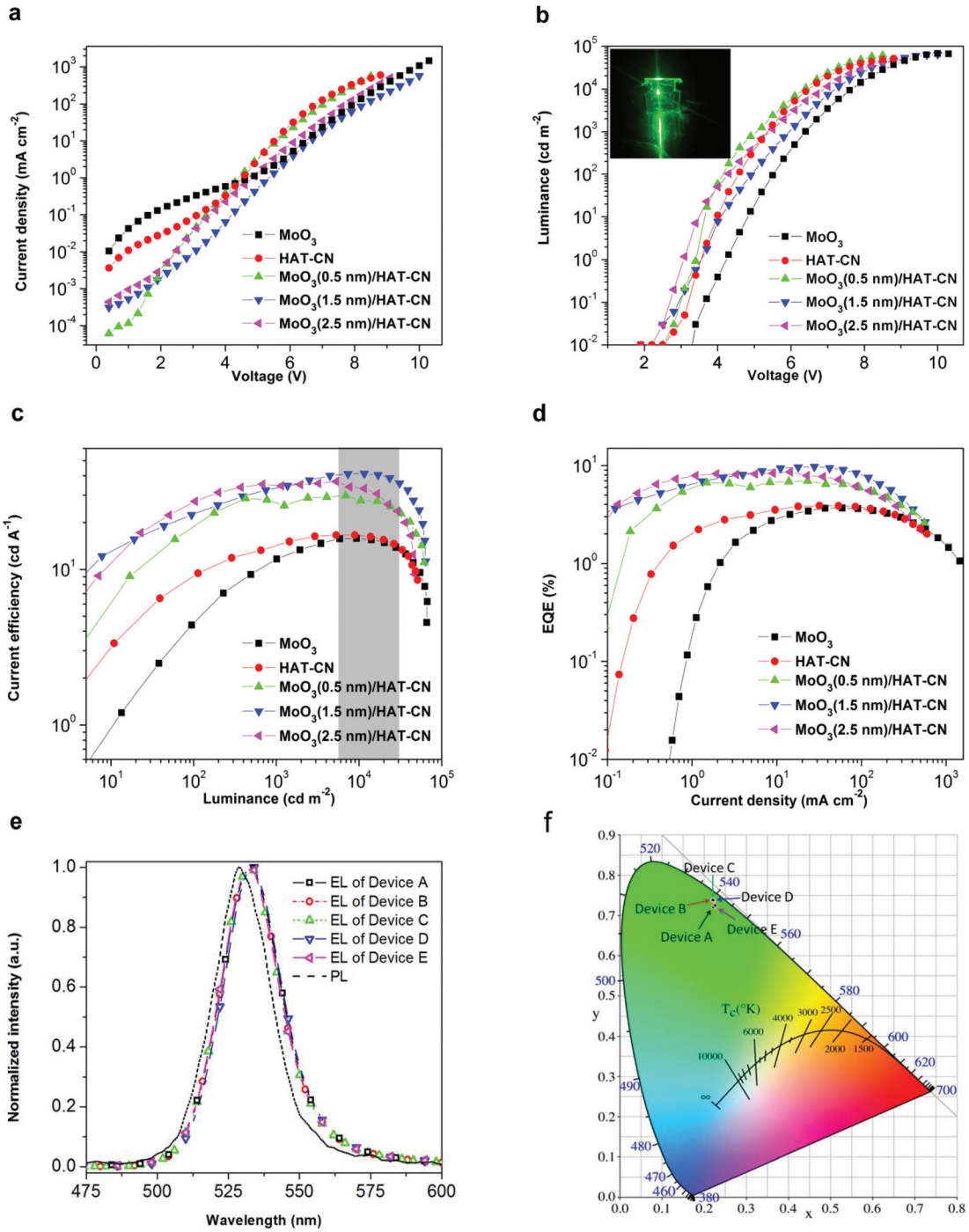

Fig. 2 EL performance of QLEDs with different HIL. (a) Current density–voltage (*J*–*V*) characteristics of QLEDs. (b) Luminance–voltage curves. Inset: Image of the device D driven under the operating voltage of 6 V. (c) CE properties as a function of luminance. (d) EQE as a function of current density. (e) Normalized PL spectrum and EL spectra of QLEDs. (f) CIE properties of device A–E.

injection current was remarkable. Current density of the hole-only devices at low driving range (<2 V) is shown in Fig. 3b. It shows that the higher the current density of a hole-only device, the lower the leakage current density of the corresponding QLED (Fig. 2a and 3b). It indicates that use of a hybrid HIL to circumvent the influence of excess electrons *via* enhancing the hole injection and transport to improve the device performance is very efficient. For the hybrid HIL device with a 2.5 nm MoO_3 layer, the current density showed slight increase than for the HAT-CN device, whereas the CE increased to 36.8 cd A^{-1} (device C) from 16.6 cd A^{-1} (device B). Thus, we suggest that even a little improvement of hole injection in QLEDs can result in effective reduction of the leakage current and this is contributed to high luminance efficiency.

Table 1 Summary of the EL characteristics of the optimized QLEDs with different HIL

Devices with different HIL	EL λ_{max} (nm)	CIE 1931	V_{on} (V)	L_{max} (cd m^{-2})	CE (cd A^{-1})		EQE (%)	
					CE_{max}	1000 cd m^{-2}	EQE_{max}	1000 cd m^{-2}
A: Single MoO_3 (4 nm)	532	(0.223, 0.722)	3.4	65 900	15.8	11.7	3.68	2.74
B: Single HAT-CN (4 nm)	532	(0.222, 0.740)	2.5	61 200	16.6	15.1	3.88	3.53
C: MoO_3/HAT-CN (0.5/2.5 nm)	532	(0.223, 0.737)	2.2	61 500	29.8	25.7	6.96	6.00
D: MoO_3/HAT-CN (1.5/2.5 nm)	532	(0.221, 0.739)	1.9	64 000	41.3	34.5	9.72	8.07
E: MoO_3/HAT-CN (2.5/2.5 nm)	532	(0.227, 0.725)	2.1	47 200	36.8	34.5	8.60	8.10

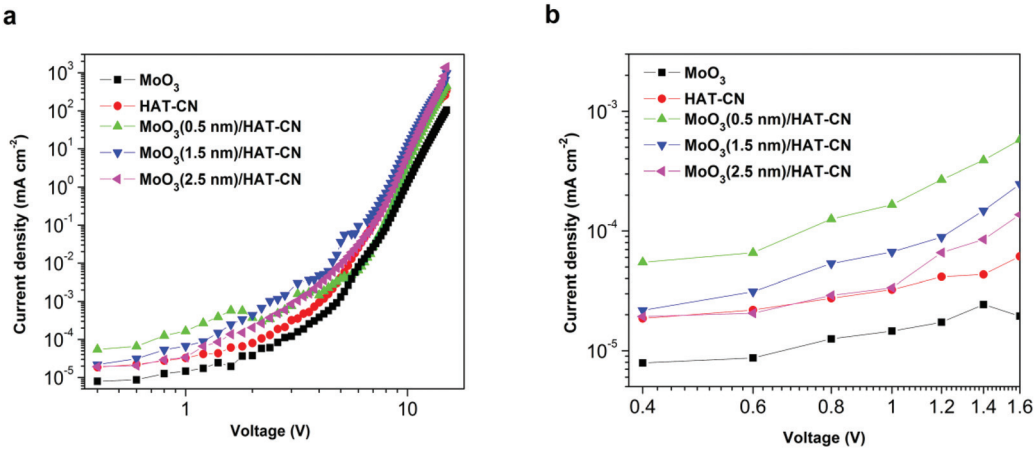

Fig. 3 Current density–voltage characteristics of the hole-only devices with different HILs. (a) *J*–*V* characteristics. (b) *J*–*V* curves in the low bias voltage range.

Devices with a structure of ITO/CBP/HIL/Al, where ITO acts as a cathode and Al as an anode, were fabricated to ensure the hole injection enhancement of the hybrid HIL device. As shown in Fig. 4a, the current density of the device with a HAT-CN HIL is much higher than that of the MoO_3 HIL device. This phenomenon appears similar when comparing the results of HAT-CN and MoO_3 HILs in an organic device.[30] Note that HAT-CN, which works as an electron acceptor layer,[31] in these devices is beneficial for hole injection. Furthermore, when the MoO_3 layer was incorporated with the HAT-CN layer, the device exhibited a great enhancement of current density. The MoO_3/HAT-CN device shows a current density of 86.4 mA cm^{-2}, over 1.34-fold higher than that of the HAT-CN device (36.8 mA cm^{-2}) at the driving voltage of 3 V.

We used the same method in OLED to calculate the injection efficiency (the calculation of the steady-state current of

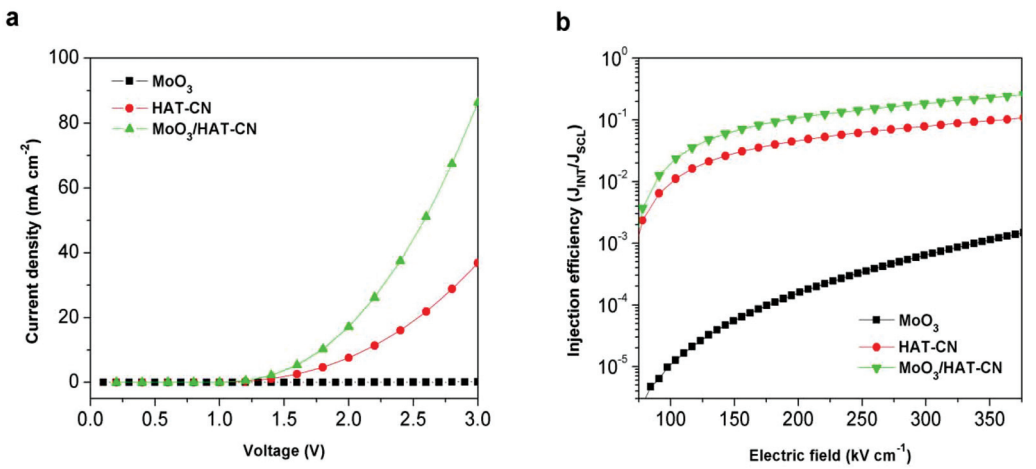

Fig. 4 (a) *J*–*V* characteristics. (b) Hole injection efficiency, J_{INT}/J_{SCL}, as a function of electric field of devices with different HIL.

the space-charge-limited current (SCLC), J_{SCL}, is provided in the ESI†). The injection efficiency η_{INJ} can be calculated from the J–V characteristics:[30]

$$\eta_{INJ} = J_{INJ}/J_{SCL} \quad (1)$$

where J_{INJ} is the measured steady-state current density and J_{SCL} is the calculated current density. The comparison of theoretical J_{SCL} with measured results is shown in the ESI (Fig. S8†). Fig. 4b shows the hole injection efficiency (η_{INJ}) curves of different HIL devices. By inserting a MoO_3 layer between HAT-CN and CBP layer, the η_{INJ} increases from 7.8% of the HAT-CN device to 18.4%, which is much larger than that of the MoO_3 device. Thus, using a thin hybrid HIL, a significant improvement of hole injection efficiency can be obtained. Moreover, the remarkable enhancement of η_{INJ} is sufficient to achieve efficient recombination of excitons as well as high-performance QLED.

Conclusions

In summary, incorporation of a hybrid MoO_3/HAT-CN interlayer into the devices was demonstrated to achieve a high hole injection efficiency. Thereby, efficient hole injection could reach a better charge balance and thus lead to an enhanced exciton recombination rate and improved EL efficiencies. The hybrid HIL in the green inverted QLEDs plays significant roles in improving the EL properties: it can enhance the hole injection ability, reduce the accumulation in space charge within the QD emitting region, and help to match the HOMO of HTLs to improve the performance of the devices. As a result, the best EL performance device with a 1.5 nm MoO_3/HAT-CN HIL exhibits a remarkable improvement of both CE and EQE, which are 1.5–1.6 fold higher than those of the devices with single HILs. A maximum CE of 41.3 cd A^{-1} and EQE of 9.72% at the current density of 27.9 mA cm^{-2}, corresponding to the luminance of 11 600 cd m^{-2}, were obtained for the best performance device. Finally, this method can be extended to other color inverted QLEDs, which would lead to bright, highly efficient, and color saturation devices for display applications.

Experimental

Materials

Potassium hydroxide was purchased from Tianjin Chemical Reagent Factory (Tianjin China). Zinc acetate dihydrate (99%) was acquired from Xilong Chemical Co., Ltd (Guangdong China). Normal butanol (99%) was purchased from Alfa-Aesar. Methanol (analytical grade) was purchased from Sinopharm Chemical Reagents (Shanghai China). CBP (99%, EL device grade) was purchased from Nichem Fine Technology Ca. Ltd. MoO_3 (99%) was purchased from Sigma Aldrich. The green emitting core–shell CdSe@ZnS QDs were provided by Mesolight Inc. with size in the range of 10–12 nm and oleic acid as the ligand. All materials were used without further purification.

Synthesis of the ZnO nanoparticles

The ZnO NPs were prepared according to a method reported in the literature.[1] Potassium hydroxide (0.74 g) dissolved in methanol (30 ml) was added dropwise to zinc acetate dihydrate (1.48 g) in methanol (60 ml) under vigorous stirring, and the reaction mixture was stirred at 60 °C for over 3.5 h. The reaction mixture was then cooled down to room temperature, and the solvent was removed from the precipitate. The precipitate was washed several times with methanol and separated by centrifugation. Subsequently, the particles were dissolved in normal butanol at a desirable concentration for our experiment.

Fabrication of the QLED

The ITO electrode glass substrates were subjected to ultrasonication in acetone, isopropanol, and deionized water for 15 min and then treated under plasma O_2 for 15 min. The treated substrates were transferred into a nitrogen-filled glove box (O_2 < 0.1 ppm and H_2O < 1 ppm). ZnO NPs (normal butanol, 30 mg ml^{-1}) and QDs (hexane, 6.5 mg ml^{-1}), were deposited layer-by-layer *via* spin coating on the substrates. The ZnO NPs layers were spin-coated at 1140 rpm for 50 s. The ZnO NPs and QDs layers were baked at 120 °C for 20 min and 90 °C for 10 min, respectively. Then, CBP, MoO_3, and HAT-CN layers were deposited using a thermal evaporation system at the deposition rates of 1–2, 0.02–0.05, and 0.08–0.18 Å s^{-1}, respectively. Finally, Al electrode (80 nm) was deposited using the same thermal evaporation system through a shadow mask under a high vacuum of 1×10^{-4} Pa. The measured devices were encapsulated with a glass lid using an UV resin.

Thickness of the multilayers in inverted QLEDs:

Device A: ITO/ZnO (35 nm)/QDs (15 nm)/CBP (50 nm)/MoO_3 (4 nm)/Al

Device B: ITO/ZnO (35 nm)/QDs (15 nm)/CBP (50 nm)/HAT-CN (4 nm)/Al

Device C: ITO/ZnO (35 nm)/QDs (15 nm)/CBP (50 nm)/MoO_3 (0.5 nm)/HAT-CN (2.5 nm)/Al

Device D: ITO/ZnO (35 nm)/QDs (15 nm)/CBP (50 nm)/MoO_3 (1.5 nm)/HAT-CN (2.5 nm)/Al

Device E: ITO/ZnO (35 nm)/QDs (15 nm)/CBP (50 nm)/MoO_3 (2.5 nm)/HAT-CN (2.5 nm)/Al

Thickness of multilayers in the hole injection devices:

MoO_3 device: ITO/CBP (150 nm)/MoO_3 (4 nm)/Al

HAT-CN device: ITO/CBP (150 nm)/HAT-CN (4 nm)/Al

Hybrid device: ITO/CBP (50 nm)/MoO_3 (1.5 nm)/HAT-CN (2.5 nm)/Al

Characterizations

Transmission electron microscopy (TEM) image was obtained *via* a Philips TECNAI G2. Atomic force microscopy (AFM) measurements were performed using a scanning probe microscope (SPM-9700, Shimadzu) in the tapping mode. Ultraviolet photoelectron spectroscopy (UPS) was carried out using the Thermo ESCALAB 250 surface analysis system. The cross-sectional scanning electron microscopy (SEM) measurements

were conducted using a field emission scanning electron microscopy instrument (S4800, Hitachi). The PL decay and absolute fluorescent quantum yield of QD solution and film on glass were measured by Edinburgh FLS920 fluorescence spectrophotometer. The PL spectrum was obtained by a fluorescence spectrophotometer (F-7000, Hitachi) under an excitation wavelength of 365 nm. The UV-vis absorption spectrum of the QD solution was obtained using a spectrophotometer (UV-3100PC, Hitachi). The thickness of the multilayers was calibrated using a surface profiler (XP-1, Ambios). The current density characteristics and luminance properties of the inverted QLEDs were measured using a system comprising a Keithley 2611 source meter together with a luminance meter (LS-110, Konica Minolta) and cross-checked with a well-calibrated spectroradiometer (PR 705, Photo Research).

Acknowledgements

This work was financially supported by the CAS Innovation Program, the National Natural Science Foundation of China (No. 61106057 and No. 11274304), the Jilin Province Science and Technology Research Project (20140912 and 20150204067GX), and the financial support was received from the State Key Laboratory of Luminescence and Applications.

References

1 J. Kwak, W. K. Bae, D. Lee, I. Park, J. Lim, M. Park, H. Cho, H. Woo, Y. Yoon do, K. Char, S. Lee and C. Lee, *Nano Lett.*, 2012, **12**, 2362–2366.
2 Y. Shirasaki, G. J. Supran, M. G. Bawendi and V. Bulović, *Nat. Photonics*, 2012, **7**, 13–23.
3 B. S. Mashford, M. Stevenson, Z. Popovic, C. Hamilton, Z. Zhou, C. Breen, J. Steckel, V. Bulovic, M. Bawendi and S. Coe-Sullivan, *Nat. Photonics*, 2013, **7**, 407–412.
4 L. Qian, Y. Zheng, J. Xue and P. H. Holloway, *Nat. Photonics*, 2011, **5**, 543–548.
5 V. Colvin, M. Schlamp and A. P. Alivisatos, *Nature*, 1994, **370**, 354–357.
6 B. N. Pal, Y. Ghosh, S. Brovelli, R. Laocharoensuk, V. I. Klimov, J. A. Hollingsworth and H. Htoon, *Nano Lett.*, 2011, **12**, 331–336.
7 J. Lim, B. G. Jeong, M. Park, J. K. Kim, J. M. Pietryga, Y. S. Park, V. I. Klimov, C. Lee, D. C. Lee and W. K. Bae, *Adv. Mater.*, 2014, **26**, 8034–8040.
8 K.-H. Lee, J.-H. Lee, H.-D. Kang, B. Park, Y. Kwon, H. Ko, C. Lee, J. Lee and H. Yang, *ACS Nano*, 2014, **8**, 4893–4901.
9 J. Kwak, J. Lim, M. Park, S. Lee, K. Char and C. Lee, *Nano Lett.*, 2015, **15**, 3793–3799.
10 Y. Yang, Y. Zheng, W. Cao, A. Titov, J. Hyvonen, J. R. Manders, J. Xue, P. H. Holloway and L. Qian, *Nat. Photonics*, 2015, **9**, 259–266.
11 H. Shen, W. Cao, N. T. Shewmon, C. Yang, L. S. Li and J. Xue, *Nano Lett.*, 2015, **15**, 1211–1216.
12 J. L. Zhao, J. A. Bardecker, A. M. Munro, M. S. Liu, Y. H. Niu, I. K. Ding, J. D. Luo, B. Q. Chen, A. K. Y. Jen and D. S. Ginger, *Nano Lett.*, 2006, **6**, 463–467.
13 Q. Lin, H. Shen, H. Wang, A. Wang, J. Niu, L. Qian, F. Guo and L. S. Li, *Org. Electron.*, 2015, **25**, 178–183.
14 A. Castan, H. M. Kim and J. Jang, *ACS Appl. Mater. Interfaces*, 2014, **6**, 2508–2515.
15 Y. Dong, J. M. Caruge, Z. Zhou, C. Hamilton, Z. Popovic, J. Ho, M. Stevenson, G. Liu, V. Bulovic and M. Bawendi, *SID Int. Symp. Dig. Tech. Pap.*, 2015, **46**, 73–75.
16 J. R. Manders, L. Qian, A. Titov, J. Hyvonen, J. Tokarz-Scott, J. Xue and P. H. Holloway, *SID Int. Symp. Dig. Tech. Pap.*, 2015, **46**, 270–273.
17 H. Peng, Y. Jiang and S. Chen, *Nanoscale*, 2016, **8**, 17765–17773.
18 H. M. Kim, J. Kim, J. Lee and J. Jang, *ACS Appl. Mater. Interfaces*, 2015, **7**, 24592–24600.
19 Y. Zou, M. Ban, W. Cui, Q. Huang, C. Wu, J. Liu, H. Wu, T. Song and B. Sun, *Adv. Funct. Mater.*, 2017, **27**, 1603325.
20 X. Dai, Z. Zhang, Y. Jin, Y. Niu, H. Cao, X. Liang, L. Chen, J. Wang and X. Peng, *Nature*, 2014, **515**, 96–99.
21 H. Zhang, N. Sui, X. Chi, Y. Wang, Q. Liu, H. Zhang and W. Ji, *ACS Appl. Mater. Interfaces*, 2016, **8**, 31385–31391.
22 W. K. Bae, J. Lim, D. Lee, M. Park, H. Lee, J. Kwak, K. Char, C. Lee and S. Lee, *Adv. Mater.*, 2014, **26**, 6387–6393.
23 H. Zhang, S. Wang, X. Sun and S. Chen, *J. Mater. Chem. C*, 2017, **5**, 817–823.
24 H.-M. Kim, J.-H. Youn, G.-J. Seo and J. Jang, *J. Mater. Chem. C*, 2013, **1**, 1567–1573.
25 H. M. Kim, D. Geng, J. Kim, E. Hwang and J. Jang, *ACS Appl. Mater. Interfaces*, 2016, **8**, 28727–28736.
26 D. Bozyigit, O. Yarema and V. Wood, *Adv. Funct. Mater.*, 2013, **23**, 3024–3029.
27 D. Bozyigit and V. Wood, *MRS Bull.*, 2013, **38**, 731–736.
28 J.-M. Caruge, J. E. Halpert, V. Bulovic and M. G. Bawendi, *Nano Lett.*, 2006, **6**, 2991–2994.
29 W. K. Woo, K. T. Shimizu, M. V. Jarosz, R. G. Neuhauser, C. A. Leatherdale, M. A. Rubner and M. G. Bawendi, *Adv. Mater.*, 2002, **14**, 1068–1071.
30 C. E. Small, S.-W. Tsang, J. Kido, S. K. So and F. So, *Adv. Funct. Mater.*, 2012, **22**, 3261–3266.
31 C.-H. Gao, X.-Z. Zhu, L. Zhang, D.-Y. Zhou, Z.-K. Wang and L.-S. Liao, *Appl. Phys. Lett.*, 2013, **102**, 153301.

